

# Chemical and isotopic signature of groundwater in the Santa Ninfa karst system and possible inferences on neotectonics

Rocco Favara<sup>1</sup>, Marianna Cangemi<sup>\*,1</sup>, Fausto Grassa<sup>1</sup>

<sup>(1)</sup> Istituto Nazionale di Geofisica e Vulcanologia, Sezione di Palermo, Palermo (Italia)

Article history: received June 25, 2019; accepted September, 4, 2019

## Abstract

The Santa Ninfa karst system is an area strongly controlled by tectonics, whose intense fracturing gave rise to the formation of a large number of cavities that foster the drainage of water. The hydrogeochemical characters of groundwater circulating in this aquifer, together with its isotopic signature, were investigated in detail. The chemistry of groundwater reflects the nature of the rocks hosting the aquifers, constituted by primary and diagenetic selenitic gypsum, salts, and gypsum-arenite, whose dissolution is responsible of the geochemical fingerprint of the quasi-totality of the samples. A single site (CAM) is characterised by a different chemical composition, indicating a mixing between Ca-sulphate, Ca-bicarbonate and a NaCl-rich water. From the chemical point of view, no evidence of interaction between shallow groundwater and deep fluids has been detected. Conversely, isotopic fluctuations highlight mixing processes between surficial (evaporated) runoff and groundwater. Different mixing proportion among these endmembers can be reflected in variations of the chemical character of the sampled springs. Changes in mixing proportions can be the effect of differential permeability variations, in turn produced by local stress field changes during seismogenic processes. In this scenario the geochemical monitoring of the Santa Ninfa karst aquifer could be of relevant interest in the study of seismogenic processes in this area, with particular reference to the relationship between seismic and geochemical transients.

Keywords: Hydrogeochemistry; Gypsum karst system; Neotectonics, Groundwater.

---

## 1. Introduction

Western Sicily is an area affected by seismicity, with several strong earthquakes that since historical times have caused relevant damages and fatalities [Guidoboni et al., 2002; Bottari et al., 2009]; the most recent catastrophic earthquake (Mw=5.6) struck the Belice Valley in 1968, destroying 7 towns and killing 330 people [De Panfilis and Marcelli, 1968; Marcelli and Pannocchia, 1971; Bottari, 1973; Anderson and Jackson, 1987; Roviola et al., 2011]. A previous study carried out in the Belice earthquake area [Favara et al., 2001a] suggested a direct connection between local thermal springs (Acqua Pia and Terme Selinuntine) and the main tectonic features, with anomalies of temperature and concentration of dissolved ions (SO<sub>4</sub>, Cl, Na, Total Dissolved Solids) and gases (CO<sub>2</sub>), in connection with the 1968 seismic sequence.

Other groundwater circulation systems in the area show evident relationships with tectonics; a very peculiar case is the aquifer of the Santa Ninfa gypsum karst system (Figure 1), located within the area struck by the 1968 seismic sequence (the town of Santa Ninfa was completely destroyed). The Santa Ninfa karst system is strongly controlled by tectonics [Madonia et al., 2017], and the intense fracturing gave rise to the formation of a large number of cavities. The largest one, namely “La Grotta”, is located at the end of a blind valley and it is a through-cave about 1350 m long and 30 m deep. It consists of at least three main levels of sub-horizontal galleries, the lowest of which is characterized by perennial flowing water, running along the water table [Madonia and Madonia, 2020].

In this study we integrated the results of the geochemical investigation published by Favara et al. [2001b] and Liotta et al. [2013] with unpublished data, with the aim of providing new insights on the hydrogeochemical characterisation of this aquifer. The hydrogeochemical system directly linked to the La Grotta hydrogeological tunnel, involving the mixing with surface runoff, is described in another paper from this volume [Madonia and Madonia, 2020]. Here we report on the general chemical and isotopic character of groundwater, paying attention to the possible inferences on neotectonics.

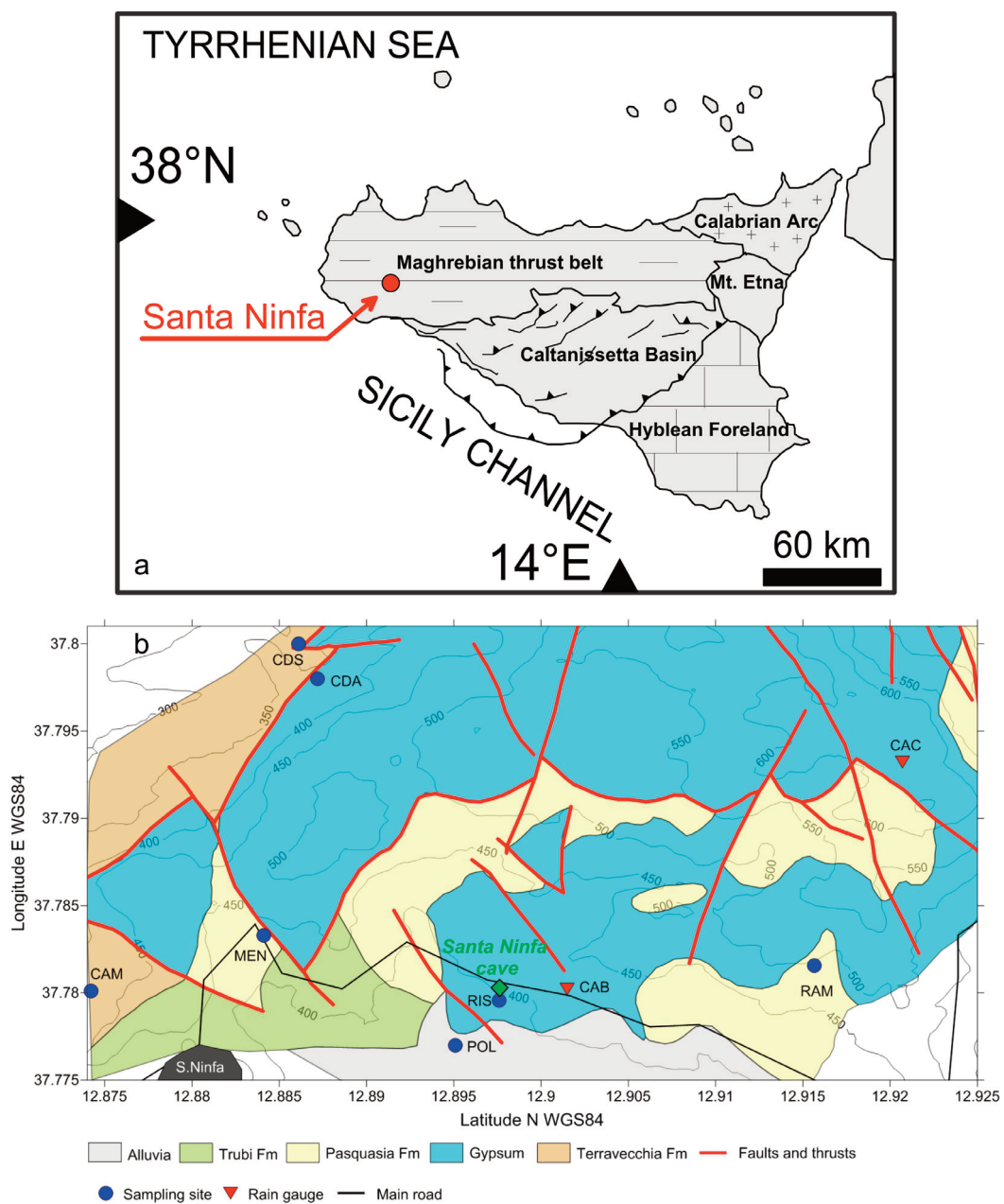


**Figure 1.** a) Geological map of Sicily; b) detailed geological map of the Santa Ninfa area (modified from Agostini and Cucchi, 1989) with locations of sampling sites (see main text for explanation of acronyms).

## 2. Study area

The study area is located in western Sicily, along the southern part of the NNW-SSE trending San Vito Lo Capo-Sciacca (SVCS) band [Di Stefano et al., 2015]. This band represents a crustal discontinuity, nearly orthogonal to the main thrust propagation of the Sicilian fold and thrust belt (SFTB), which separates two zones showing a different Permian to Tertiary evolution: thick carbonate platforms in the western sector, facing deep-water successions located in the eastern one. Upper Triassic reefs, huge megabreccia, and submarine volcanism suggest the existence of a long-lasting weakness zone, related to this discontinuity and located at the boundary between its western and eastern sectors. This discontinuity has been episodically reactivated with transpressional and/or transtensional mechanisms [Di Stefano et al., 2015]. The historical and recent seismicity of the area identifies western Sicily as an active deformation zone; the strongest seismic activity was recorded in 1968 (Belice seismic sequence, maximum  $M_w=5.6$ ). A previously unknown Quaternary fault was identified at Monte Porcello [MPF; Michetti et al., 1995], showing geometry and kinematics consistent with a regional NNW-SSE trending, right-lateral strike-slip zone. The MPF, together with other adjacent faults, crosscuts upper Piacenzian to Gelasian calcarenites and clays, and accommodates the differential shortening of the large-ramp anticline (Gibellina anticline) formed by Tortonian to lower Pliocene sediments [Di Stefano et al., 2015].

The studied area of the Santa Ninfa gypsum karst system lies immediately NW of MPF, inside the Castelvetro Basin. Its sedimentary succession is composed of: i) upper Tortonian terrigenous and carbonate-clastic sediments (Terravecchia Fm); ii) lower Messinian evaporite deposits (Gessoso-Solfifera Series, including the Pasquasia Fm) composed of evaporitic limestones, primary and diagenetic selenitic gypsum, salts, gypsum-arenites, and greyish marly clay; iii) lower Pliocene globigerinid chalky-limestone (Trubi Fm); iv) middle-upper Pliocene marly arenaceous sands (Santa Margherita Belice Fm) [Basilone, 2012].

The surficial hydrography is mainly constituted by epigeic karst landforms (e.g. dolines and blind valleys) from which precipitations funnel into the underground feeding the aquifer.

Thermometric and pluviometric data recorded from 1951 to 1986 in 3 different local meteorological stations reveal an average annual temperature of 15.9° C, which hottest month is August (average monthly temperature of 25.6° C), whereas January is the coldest one (9.4° C average monthly temperature). The average annual rainfalls account for 584 mm and are distributed in 73 days, with the wettest month in December (87 mm) and the driest in July (6 mm). Following the abovementioned seasonal distributions of air temperature and rainfall, the climate of the Santa Ninfa area can be classified as temperate-semiarid.

This area is characterised by well-developed karst phenomena, both at the surface and underground. Their formation is linked to the presence of both tectonic dislocations and impermeable levels that foster the drainage of water through preferential flow pathways [Madonia and Panzica La Manna, 1987]. The hydrogeological setting of the studied area is characterised by an impermeable substrate constituted by clay of Terravecchia Fm, covered by Messinian gypsum that constitutes the main reservoir.

## 3. Analytical methods

This study is based on data acquired in different periods during the last 20 years. Six springs Rampinzeri, Risorgenza, Polla, Case Di Stefano, Capo D'Acqua and Case Monreale (hereafter referred as RAM, RIS, POL, CDS, CDA and CAM, respectively) were collected every three months, from April 1997 to May 1998. During the same period, isotopic composition of rainfall was measured in samples collected in two rain-gauges, located at 430 m and 630 m a.s.l. (sites Case Biondo and Case Catalano, CAB and CAC, respectively). Other isotopic data of precipitation (SNI), related to the period 2004-06, are from the study of Liotta et al. [2013]; additional chemical data from another spring (MEN) were collected in 2014. Location of sampling sites is shown in Figure 1b.

Chemico-physical parameters (pH and electric conductivity) were measured directly in the field using Orion instruments. Water samples used for the determination of dissolved major and trace elements were first filtered using 0.45 µm Millipore MF filter and then collected in LD-PE (low-density polyethylene) bottles for major element analyses, acidifying to ca pH 2 the aliquot destined to cation determination with HCl. Untreated aliquots were stored for alkalinity determinations, made via titration with HCl (0.1 N). Major ions were determined by ionic chromatography using Dionex 2000i. Major elements data are presented in Table 1. All measured values

were processed using the computer program PHREEQC, version 3.1.2, [Parkhurst & Appelo, 2013], in order to calculate ion activities and  $PCO_2$  (partial pressure of  $CO_2$ ) of the water samples, as well as saturation state with respect to relevant minerals.

The O and H isotopic compositions of groundwater and rain samples were determined using Analytical Precision AP 2003 and FinniganMAT Delta Plus IRMS devices, respectively. The isotopic ratios are expressed as the deviation per mil ( $\delta$  ‰) from the international standard V-SMOW. The uncertainties are  $\pm 0.1\%$  for  $\delta^{18}O$  and  $\pm 1\%$  for  $\delta D$ .

Contour maps were realised using the kriging algorithm implemented in the contouring options of Golden Software Surfer release 16; we adopted the blanking option for grid points outside the convex hull of data, for avoiding the generation of extrapolated information outside the area covered by measures.

Sample	Date	T	pH	EC	Na	K	Mg	Ca	Cl	SO <sub>4</sub>	HCO <sub>3</sub>	TDS
RAM	Apr 97	16.8	7.07	1862	2.02	0.140	2.29	16.1	2.48	17.3	4.00	2775
RAM	Jul 97	18	7.13	1734	2.00	0.070	3.08	16.6	2.26	16.7	4.60	2777
RAM	Sep 97	17.9	7.00	816	2.20	0.04	2.57	18.1	1.59	19.2	4.00	3003
RAM	Nov 97	16.5	6.85	1962	3.20	0.110	2.67	17.5	2.25	16.6	4.70	2832
RAM	Feb 98	18.1	7.08	2050	1.06	0.030	1.9	17.7	3.25	16.5	4.30	2787
RAM	Mar 98	17.0	6.90	950	1.79	0.05	2.15	16.9	1.04	18.0	4.20	2812
RAM	May 98	17.3	7.03	1902	2.07	0.009	2.48	17.0	2.56	16.8	4.40	2791
RIS	Apr 97	15.6	7.06	1965	3.75	0.140	2.91	17.1	2.29	17.7	3.80	2895
RIS	Jul 97	18.6	6.3	2020	4.23	0.009	3.86	16.2	3.69	17.3	4.30	2919
RIS	Nov 97	16.3	7.62	1454	4.78	0.200	3.06	17.3	3.06	19.0	4.00	3081
RIS	Feb 98	16.2	7.41	2230	3.04	0.140	2.29	17.6	4.08	16.8	4.10	2888
RIS	May 98	17.1	7.35	1917	3.95	0.140	3.03	17.1	3.28	17.7	4.10	2949
POL	Apr 97	17	7	2110	4.74	0.170	2.96	17.2	4.26	17.6	4.90	3059
POL	Jul 97	18.5	6.92	2060	4.38	0.220	3.17	16.2	3.85	16.5	5.10	2905
POL	Nov 97	16.7	6.99	1454	5.70	0.160	2.92	18.3	3.64	18.5	5.50	3217
POL	Feb 98	22.2	7.05	2660	4.83	0.210	2.68	18.4	4.05	18.9	4.80	3210
POL	May 98	18.2	6.99	2071	4.91	0.190	2.93	17.5	3.95	17.9	5.10	3098
CDS	Apr 97	15.8	7.26	1946	3.14	0.050	2.43	16.6	2.45	17.4	3.30	2765
CDS	Jul 97	17	6.98	2140	4.05	0.080	3.72	17.7	3.50	18.7	4.20	3088
CDS	Nov 97	16.5	7.38	1498	5.04	0.170	2.75	17.5	3.91	17.3	4.70	3001
CDS	Feb 98	19.9	7.68	2320	2.18	0.180	2.19	18.0	6.32	15.9	3.50	2868
CDS	May 98	16.2	7.33	1976	3.60	0.120	2.77	17.5	4.05	17.3	3.90	2926
CDA	Apr 97	14.6	7.9	1790	2.88	0.080	1.71	16.4	3.29	17.0	2.40	2702
CDA	Nov 97	14.6	7.84	1410	3.56	0.080	1.86	17.5	2.70	17.8	3.00	2839
CDA	Feb 98	20.7	7.94	2230	2.32	0.040	1.44	17.1	2.92	17.7	2.50	2753
CDA	May 98	15.2	7.89	1810	2.92	0.070	1.67	17.0	2.97	17.5	2.60	2766
CAM	Apr 97	13.3	7.07	776	2.37	0.730	0.640	2.19	3.13	0.855	2.90	600
CAM	Jul 97	21.3	7.47	877	2.65	0.900	0.655	1.09	2.34	0.635	2.90	493
CAM	Nov 97	16.8	7.01	821	2.90	0.810	0.675	2.26	2.41	0.645	5.20	689
CAM	Feb 98	15.9	7.05	801	2.13	0.780	0.355	2.33	2.29	0.660	6.10	717
CAM	May 98	14.9	7.15	819	2.51	0.810	0.580	2.18	2.54	0.700	4.30	633
CAM	Oct 14	21.4	7.43	956	2.53	0.710	0.675	2.77	2.18	0.82	6.10	753.01
MEN	Oct 14	18.0	7.16	2670	2.65	0.29	1.18	15.5	2.37	15.0	3.30	2775

## S. Ninfa aquifer: geochemical signature

Sample	Date	SI calcite	SI dolomite	SI gypsum	SI anhydrite	PCO <sub>2</sub>	δ <sup>18</sup> O	δD
RAM	Apr 97	3.84E-01	-5.65E-02	1.47E-02	-1.72E+00	-1.72E+00	-6.4	-35
RAM	Jul 97						-6.2	-32
RAM	Sep 97	2.69E-01	-2.59E-01	2.30E-02	-1.44E+00	-1.44E+00		
RAM	Nov 97	4.90E-01	4.96E-02	2.90E-02	-1.70E+00	-1.70E+00	-6.7	-37
RAM	Feb 98							
RAM	Mar 98	4.18E-01	3.08E-02	1.82E-02	-1.64E+00	-1.64E+00		
RAM	May 98						-6.2	-35
RIS	Apr 97	3.56E-01	-5.12E-02	3.73E-02	-1.75E+00	-1.75E+00	-6.3	-36
RIS	Jul 97	-3.30E-01	-1.24E+00	-6.68E-03	-9.15E-01	-9.15E-01	-6.1	-30
RIS	Nov 97	9.32E-01	1.13E+00	5.60E-02	-2.29E+00	-2.29E+00	-6.4	-32
RIS	Feb 98	7.62E-01	6.54E-01	3.00E-02	-2.06E+00	-2.06E+00		
RIS	May 98	6.93E-01	6.63E-01	2.81E-02	-2.00E+00	-2.00E+00	-5.9	-32
POL	Apr 97	4.23E-01	1.07E-01	2.27E-02	-1.57E+00	-1.57E+00	-6.3	-40
POL	Jul 97	3.66E-01	6.85E-02	-1.84E-02	-1.46E+00	-1.46E+00	-5.9	-34
POL	Nov 97	4.77E-01	1.76E-01	5.88E-02	-1.51E+00	-1.51E+00	-6.2	-34
POL	Feb 98	5.30E-01	3.11E-01	5.36E-02	-1.58E+00	-1.58E+00		
POL	May 98	4.52E-01	1.68E-01	3.11E-02	-1.54E+00	-1.54E+00	-6	-37
CDS	Apr 97	4.90E-01	1.54E-01	3.21E-02	-2.01E+00	-2.01E+00		
CDS	Jul 97	3.41E-01	3.19E-02	4.91E-02	-1.62E+00	-1.62E+00	-6.4	-32
CDS	Nov 97	7.86E-01	7.87E-01	2.90E-02	-1.97E+00	-1.97E+00	-6.3	-32
CDS	Feb 98	1.02E+00	1.19E+00	7.45E-03	-2.39E+00	-2.39E+00	-6.3	-35
CDS	May 98	6.53E-01	5.22E-01	3.38E-02	-2.01E+00	-2.01E+00	-6.4	-33
CDA	Apr 97	9.60E-01	9.30E-01	3.09E-02	-2.80E+00	-2.80E+00	-6.6	-31
CDA	Nov 97	1.02E+00	1.05E+00	6.14E-02	-2.65E+00	-2.65E+00		
CDA	Feb 98	1.11E+00	1.21E+00	3.88E-02	-2.80E+00	-2.80E+00	-6.5	-38
CDA	May 98	1.00E+00	1.00E+00	4.82E-02	-2.76E+00	-2.76E+00	-6.3	-31
CAM	Apr 97	-3.45E-01	-1.26E+00	-1.64E+00	-1.83E+00	-1.83E+00		
CAM	Jul 97	-1.01E-01	-3.39E-01	-2.02E+00	-2.18E+00	-2.18E+00	-6.3	-35
CAM	Nov 97	-9.12E-02	-6.86E-01	-1.76E+00	-1.50E+00	-1.50E+00	-6.1	-29
CAM	Feb 98	1.84E-02	-7.74E-01	-1.73E+00	-1.47E+00	-1.47E+00	-5.9	-28
CAM	May 98	-7.00E-02	-7.25E-01	-1.72E+00	-1.73E+00	-1.73E+00		
CAM	Oct 14	3.56E-01	-5.12E-02	3.73E-02	-1.75E+00	-1.75E+00	-6.2	-33
MEN	Oct 14	4.14E-01	-2.55E-01	-3.15E-02	-1.89E+00	-1.00E+02		

**Table 1.** Temperature (°C), pH, electrical conductivity (EC, μS cm<sup>-1</sup>), major element concentrations (mmol L<sup>-1</sup>), Total Dissolved Solids (TDS (expressed in mg L<sup>-1</sup>), saturation indexed (SI) of calcite, dolomite, gypsum and anhydrite, CO<sub>2</sub> partial Pressure (PCO<sub>2</sub> in atm) and isotopic compositions of groundwater. The δ<sup>18</sup>O and δD values are expressed in ‰ versus V-SMOW.

## 4. Results

### 4.1 Chemico-physical parameters, concentration of major elements of groundwater

Chemico-physical parameters and the results of the chemical analyses are listed in Table 1. Values of pH, temperature and electrical conductivity range between 5.83 and 7.95, 12.4 and 24.6° C, 776 and 3430  $\mu\text{S cm}^{-1}$ , respectively.

The data are also presented in the ternary diagrams of the main anions and cations (Figure 2a-b). The quasi totality of samples falls close to the  $\text{SO}_4$ -corner, whereas CAM samples show a more scattered distribution close to the  $\text{HCO}_3^-$ -corner; in the ternary cations diagram data fall close to the Ca-corner. Total Dissolved Solids (TDS) show the lowest values in sample CAM (<500  $\text{mg L}^{-1}$ ) and range from 493 to 3217  $\text{mg L}^{-1}$  in the first group, showing their maximum values in SUL.

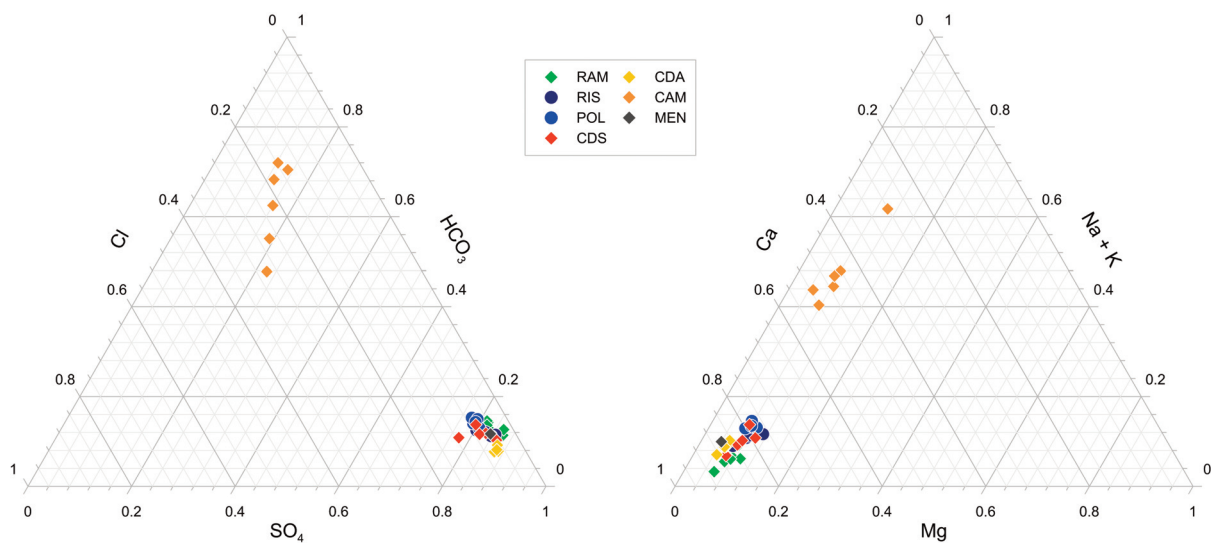


**Figure 2.** Ternary diagram of main anions.

The scatter plots reported in Figure 3 correlate the molar abundance of Na vs Cl,  $\text{SO}_4$  vs Ca and  $\text{HCO}_3^-$  vs Ca/ $\text{SO}_4$ . In the Na vs Cl diagram (Figure 3a) samples fall close to the line representative of halite mainly due to dissolution processes of evaporite minerals, with some points showing Na or Cl excess probably related to ion-exchange reactions between water and clay minerals [Martin et al., 1996].

The  $\text{SO}_4$  vs Ca scatterplot (Figure 3b) reveals that all samples belonging to the first group show both  $\text{SO}_4$  and Ca concentrations above 30  $\text{meq L}^{-1}$  and a stoichiometric ratio close to that one of the gypsum. CAM samples are characterised by  $\text{SO}_4$  and Ca concentrations below 10  $\text{meq L}^{-1}$  and variable Ca/ $\text{SO}_4$  ratio. In the  $\text{HCO}_3^-$  vs Ca/ $\text{SO}_4$  scatter plot (Figure 3c) samples belonging to the first group fall along a line, parallel to the ordinate axis, whereas CAM samples deviate from this alignment and are more enriched in Ca concentration with respect to sulphate.

Saturation indexes of the main mineralogical phases are plotted in Figure 4. Most of the samples are oversaturated in calcite, dolomite and gypsum, with the exception of MEN that is undersaturated in dolomite, and CAM in dolomite and gypsum.

## S. Ninfa aquifer: geochemical signature

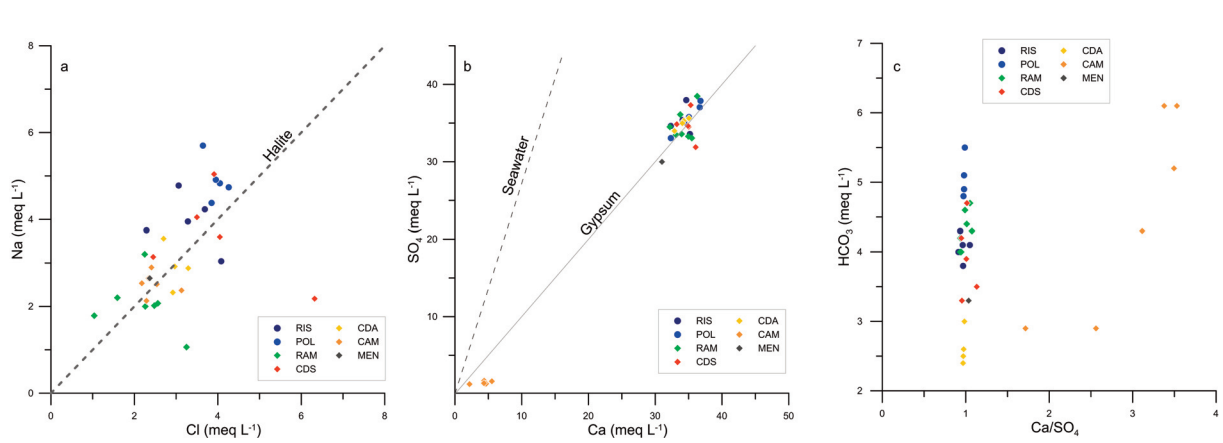


**Figure 3.** Scatter plots of: a) Na vs Cl b)  $\text{SO}_4$  vs Ca; c)  $\text{HCO}_3$  vs  $\text{Ca}/\text{SO}_4$ .

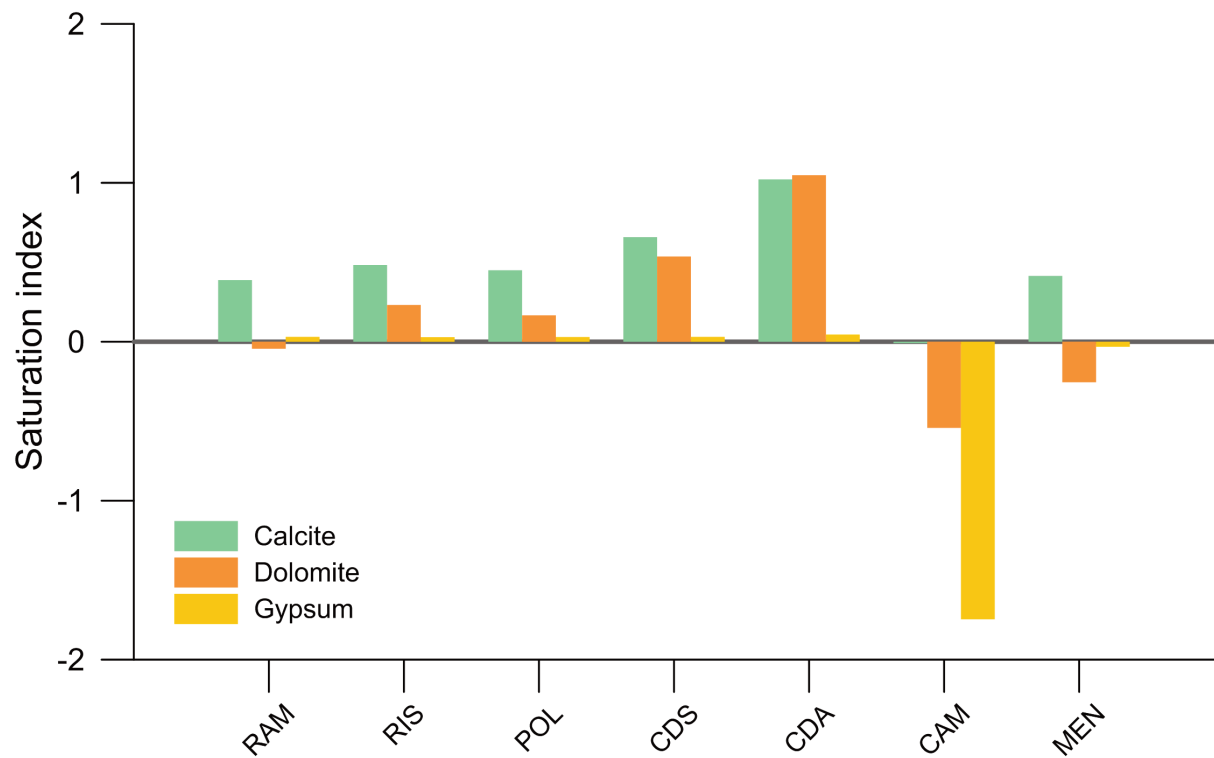


**Figure 4.** Saturation index diagram of the main mineralogical phases.

### 4.2 Isotopic composition of precipitation and groundwater

The oxygen isotopic composition of rainwater, illustrated in Fig. 5a-b, shows a large variability, with a minimum of  $-9.54\text{‰}$  (SNI, December 2005) and a maximum of  $-2.5\text{‰}$  (SNI, August 2005);  $\delta\text{D}$  spans from  $-60$  to  $-11\text{‰}$  recorded in the same site and months.

The isotopic composition of groundwater (Figure 5a-b) shows a lower range of variability, with  $\delta^{18}\text{O}$  from  $-6.7$  to  $-5.9\text{‰}$  and  $\delta\text{D}$  from  $-40$  to  $-30\text{‰}$ .

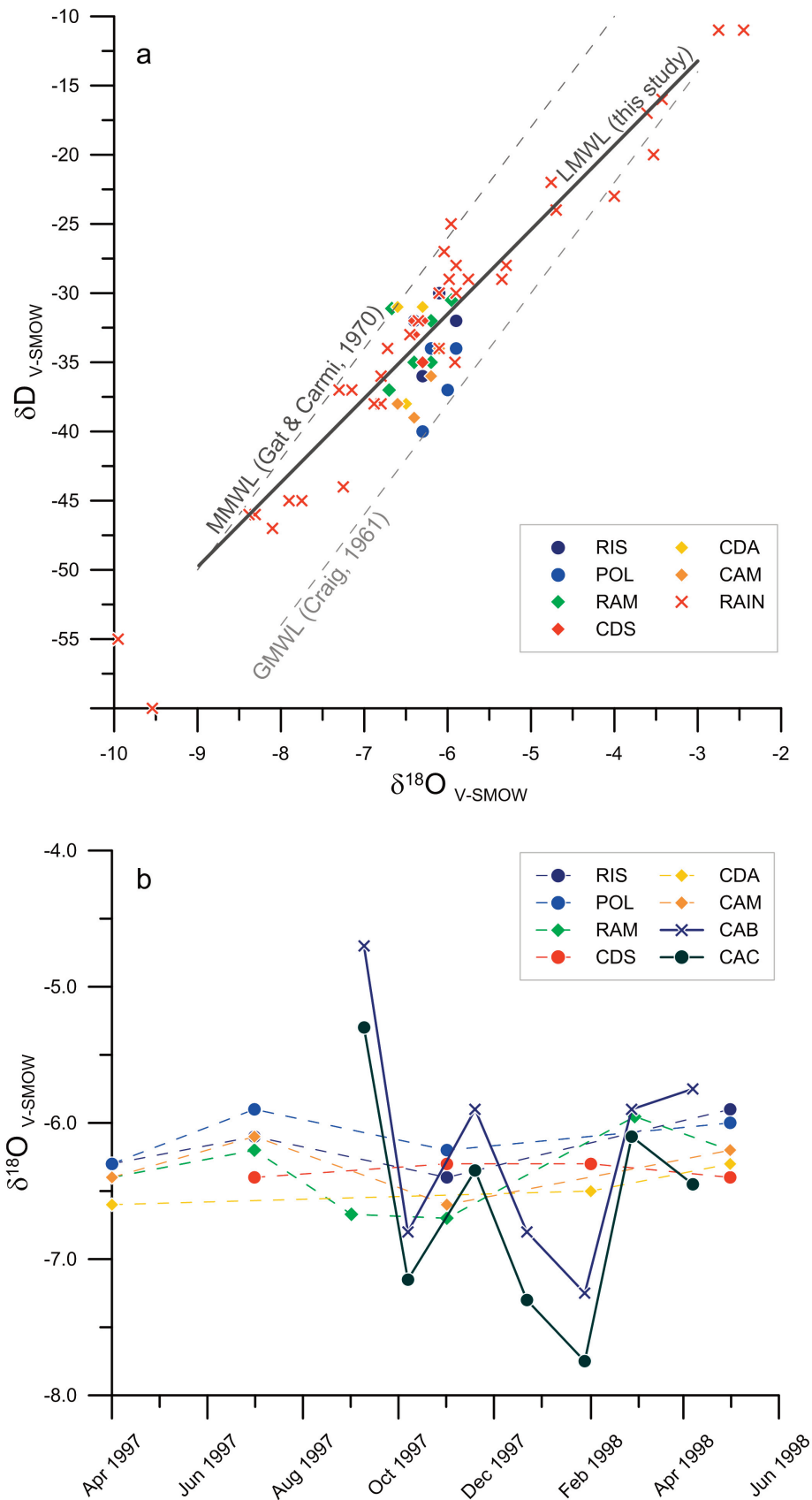


**Figure 5.** a) Oxygen and deuterium composition of groundwater and meteoric water. Grey dashed lines represent the Global Meteoric Water Line (GMWL, Craig, 1961) and Mediterranean Meteoric Water Line (MMWL, Gat and Carmi, 1970). Black line represents the Local Meteoric Water Line (LMWL); b) temporal variation of oxygen isotopic composition of rain water and groundwater and their relationship.

## 5. Discussion

### 5.1 Chemico-physical character of groundwater

The observed geochemical differences between CAM and all other samples can be explained by the distinctive nature of the rocks hosting the aquifers. These are mainly constituted by primary and diagenetic selenitic gypsum, salts, and gypsum-arenite (Gessoso Solifera Series), whose dissolution is responsible of the geochemical fingerprint of the quasi-totality of the samples. The site CAM is characterised by a different chemical character, indicating a mixing between Ca-sulphate, Ca-bicarbonate and a NaCl-rich water. CAM is located in the Terravecchia Fm, composed of terrigenous and carbonate-clastic sediments, that is sited stratigraphically below the Gessosa Solifera Fm, from which it receives groundwater enriched in both sulphate and NaCl. During the hydrologic cycle CAM shows fluctuations, with the gypsum component prevailing on the bicarbonate one and vice versa.

Saturation indexes of the first group of groundwater reveal that all samples are saturated with respect to gypsum, and quite all of them are oversaturated in carbonate minerals (both calcite and dolomite). CAM samples are undersaturated with respect to both carbonates and gypsum.

### 5.2 Isotope hydrology and reconstruction of hydrogeological circuits

The isotopic composition of rainwater shows a large range of values, mainly due to the high seasonal variability that reflects the climatic features of the Mediterranean area (Figure 5a). The best fitting line in the diagram  $\delta D$  vs  $\delta^{18}O$  represents the local meteoric water line (LMWL), calculated in this study, described by the equation:  $\delta D = 6.09 \delta^{18}O + 5.05$ . As expected, the most negative values were recorded during the cold months and conversely the less negative during the warm dry-season. The calculated LMWL is comprised between the Global [Craig, 1961] and the Mediterranean (Gat and Carmi, 1970) Meteoric Water Lines.

The isotopic vertical gradient can be computed using data from CAC and CAB but excluding SNI, because this site operated in a different period: its value ( $\delta^{18}O$ ) is  $-0.12 \delta \text{‰}/100 \text{ m}$ , lower than that found by Longinelli and Selmo [2003] for southern Italy ( $-0.2 \delta \text{‰}/100 \text{ m}$ ) but equal to that found by Liotta et al. [2013] for western Sicily.

The time distribution of isotopic compositions of groundwater (Figure 5b) presents, as expected, minor fluctuations with respect to rain, with a range of less than  $1 \delta \text{‰}$  for  $\delta^{18}O$ . In particular, the most variable is RAM ( $0.8 \delta \text{‰}$ ) while the most constant is CDS ( $0.1 \delta \text{‰}$ ); all the others exhibit a range of  $0.3\text{--}0.5 \delta \text{‰}$ . The smoothed isotopic signal recorded in groundwater suggests that: i) no direct connections between sinkholes absorbing surface runoff and the main aquifer exist, and ii) the average residence time of groundwater is close to one hydrologic year. The relationships between the isotopic signal and the hydrogeologic circuit are well evidenced in Figure 6, where the isotopic composition contour map of groundwater is reported. The most variable spring is RAM, which is located at the highest altitude (487 m a.s.l.); this spring is the emergence point of a perched aquifer characterised by a thin hydrogeologic circuit (about 180 m, considered that the maximum elevation is Mt Finestrelle, 660 m high). The second more variable site is CAM ( $0.5 \delta \text{‰}$ ), which is also the second highest (421 m a.s.l.) with a maximum thickness of the hydrogeological circuit of 240 m; the water body feeding this spring probably is a perched aquifer as the previous one. All the other springs (CDA, CDS, RIS and POL) are related to the basal aquifer, but they show a different time variability. The most constant is CDS ( $0.1 \delta \text{‰}$ ), located in the northern part of the area and intersected by a tectonic discontinuity, as the close CDA showing a low variability ( $0.3 \delta \text{‰}$ ). The other two springs, RIS and POL, are located in the southern margin of the gypsum outcrop and exhibit a slightly higher variability ( $0.4 \delta \text{‰}$ ); this is not surprising because these springs are a part of the karst hydrogeological system of La Grotta, where recurrent inputs of surface runoff interact with the basal flow [Madonia and Madonia, 2020]. The contribution of evaporated surface runoff is further confirmed by the comparison between the average isotopic composition of groundwater and the mean yearly composition of rain, weighted for rainfall amount (Table 2). We can distinguish between two different groups. The first one includes the sites whose isotopic composition is comprised between those of the two rain gauges: CDA, RAM, CDS, CAM and MEN. This behaviour is compatible with aquifers fed by local rain. The second group is composed of sites (RIS and POL) showing an isotopic composition more positive than that of the rain gauge located at the lowest altitude (CAB). This apparent discrepancy can be explained by the contribution of evaporated surface runoff, absorbed by the Biviere sinkhole and mixing with the basal aquifer flow.

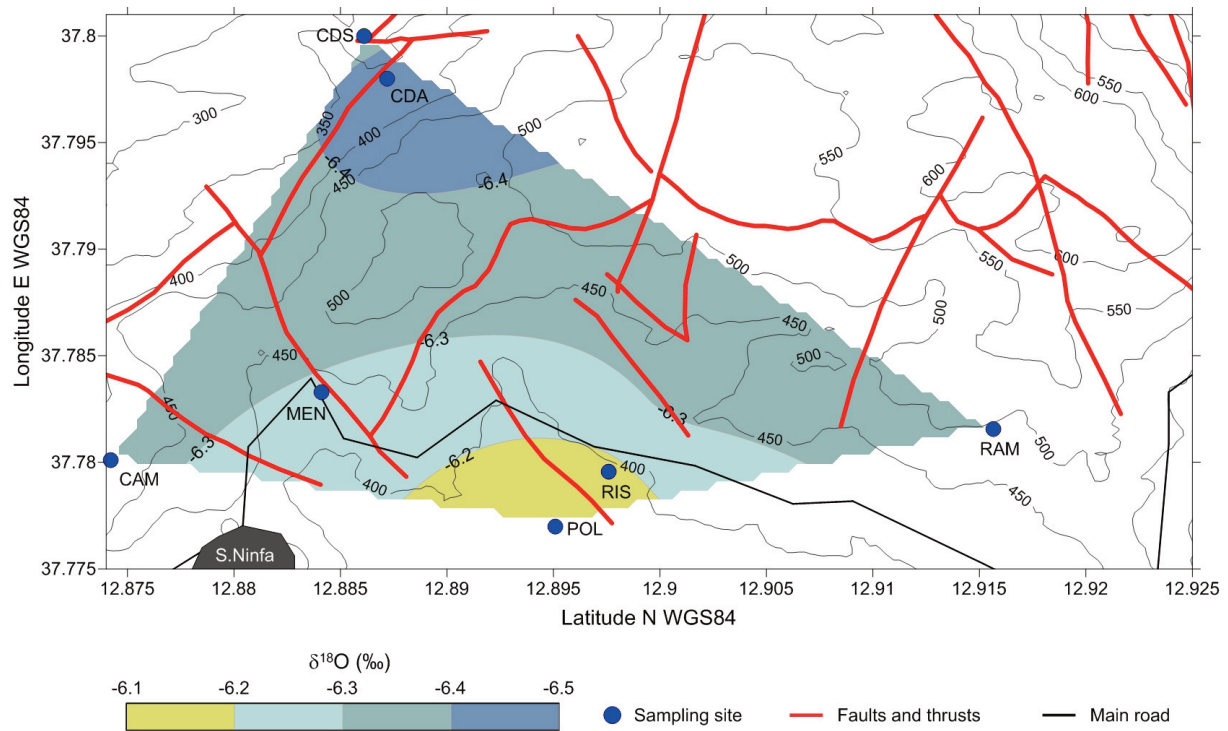


**Figure 6.** Spatial distribution of oxygen isotopic composition of groundwater.

Sample	Altitude (m asl)	Weighted mean $\delta^{18}\text{O}$
CDA	367	-6.47
RAM	487	-6.35
CDS	323	-6.35
CAM	421	-6.33
RIS	414	-6.18
POL	362	-6.10
CAB	430	-6.22
CAC	635	-6.30

**Table 2.** Weighted mean  $\delta^{18}\text{O}$  compositions of groundwater and meteoric water.

Another clue of different hydrogeological circuits characterising the two groups of springs above discussed is given by the spatial distribution of partial pressure of dissolved  $\text{CO}_2$  ( $PCO_2$ , Figure 7). The behaviour of the contour lines highlights an anomaly centred on RIS and POL that interrupts its flat spatial distribution. The origin of the dissolved  $\text{CO}_2$  in these springs is organic, as suggested by its  $\delta^{13}\text{C}$  value calculated from the composition of the total dissolved inorganic carbon in RIS and POL:  $-21$  and  $-22$  ‰, respectively (INGV, Sezione di Palermo – internal database). The higher dissolved  $\text{CO}_2$  values measured in samples from La Grotta hydrogeological system are due to the higher residence time, and consequent higher chemical maturity, of groundwater representing the local basal flow that circulates in this cave. Surface runoff drained underground by absorbing caves and smaller karst cavities transports huge amounts of suspended organic particular matter, which is accumulated in the small size karst discontinuities and fractures where groundwater flow is very slow or static. The following degradation of organic matter produces  $\text{CO}_2$  that is drained by karst conduits of larger size, like the La Grotta system.

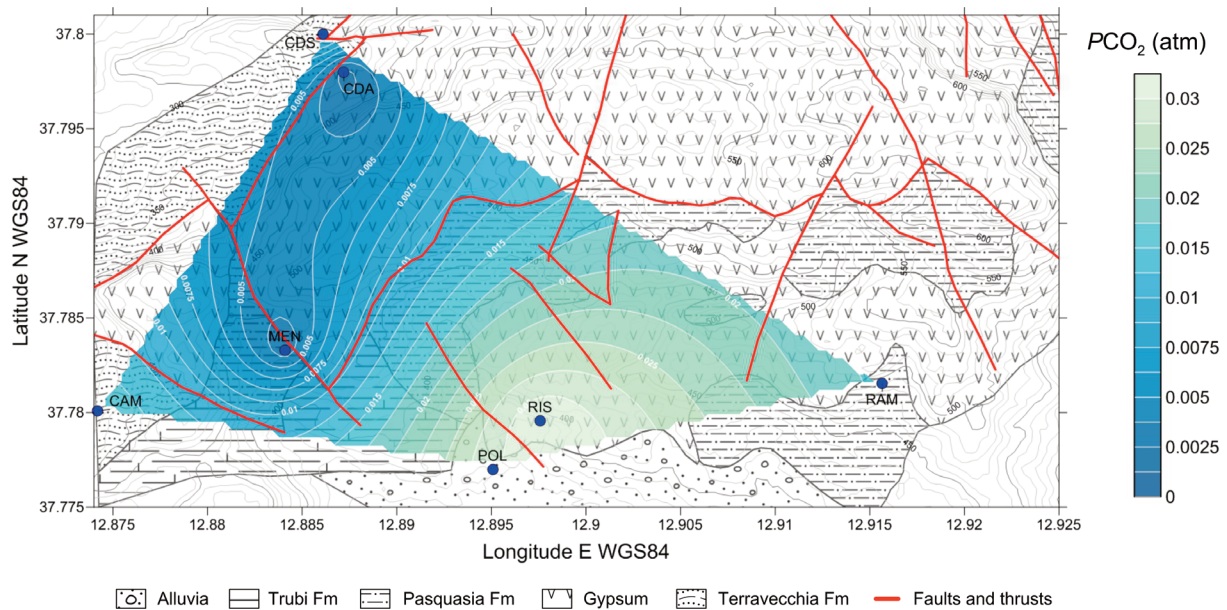


Figure 7.  $PCO_2$  of groundwaters and location of the main structural-tectonic features of the area.

This interpretation is supported by the values of soil  $CO_2$  flux measured in a transect crossing the surface projection of the main gallery of La Grotta, which are lower ( $4 \text{ g m}^{-2} \text{ d}^{-1}$ ) over the gallery and higher ( $162 \text{ g m}^{-2} \text{ d}^{-1}$ ) on both sides [Camarda et al., 2020].

## 6. Hydrogeochemical characters and possible inferences on neotectonics

Our results highlight the lack of mixing processes between shallow groundwater and deep fluids. The study of this aquifer does not provide results useful as proxies for neotectonics processes involving circulation of deep fluids. Conversely, mixing processes between surficial (evaporated) and groundwater occur, as evidenced by isotopic variations with time. Studies on seismogenic areas [i.e. Favara et al., 2007; Madonia et al., 2013] highlighted that the variation in the stress fields during neotectonic activity cause permeability variations. The dynamics of the local stress field during seismic phase seemingly induces differential permeability variations, closing fractures (i.e. reducing permeability) in sub-volume interested by compression and, conversely enhancing permeability where tension prevails [Favara et al., 2007]. Stress-induced permeability changes can result in variations of geochemical parameters [Favara et al., 2007], especially in multicomponent aquifers, like the Santa Ninfa aquifer; these variations can result in different mixing proportion among the different endmembers. Therefore, the monitoring of such a system could be of relevant interest for the earthquake forecasting, using geochemical parameters for detecting anomalies of the crustal stress dynamics.

## References

- Agostini, S. and F. Cucchi (1989). Caratteristiche geologiche dell'area di Santa Ninfa. In: "I Gessi di Santa Ninfa (Trapani). Studio multidisciplinare di un'area carsica". Memorie dell'Istituto Italiano di Speleologia – 3 – Serie II. EDS. Agnesi, V., Macaluso, T., Palermo, 204 p.
- Anderson, H. and J. Jackson (1987). Active tectonics of the Adriatic Region. *Geophys. J. R. Astr. Soc.*, 91, 937-983.
- Basilone, L. (2012). Litostratigrafia della Sicilia. ARTA (Reg. Sicil.) - ORGS, Arti Grafiche Palermitane s.r.l., Palermo, 160.
- Bottari, A. (1973). Attivita sismica e neotettonica della Valle del Belice. *Ann. Geophys.* XXVI (1), 55-84.
- Bottari, C., S.C. Stiros and A. Teramo (2009). Archaeological evidence for destructive earthquakes in Sicily between

- 400 B.C. and A.D. 600. *Geoarchaeology*, 24 (2), 147-175, <http://dx.doi.org/10.1002/geo.20260>.
- Camarda, M., S. De Gregorio, R.M.R. Di Martino, R. Favara, V. Prano (2020). Relationships between soil CO<sub>2</sub> flux and tectonics structures in SW Sicily. This volume
- De Panfilis, M. and L. Marcelli (1968). Il periodo sismico della Sicilia occidentale iniziato il 14 gennaio 1968. *Ann. Geophys.*, XXI (4), 343-421.
- Di Stefano, P., R. Favara, D. Luzio, P. Renda, M.S. Cacciatore, M. Calò, G. Napoli, L. Parisi, S. Todaro and G. Zarcone (2015). A regional-scale discontinuity in western Sicily revealed by a multidisciplinary approach: A new piece for understanding the geodynamic puzzle of the southern Mediterranean. *Tectonics*, 34, 2067-2085, doi: 10.1002/2014TC003759.
- Favara, R., F. Grassa, S. Inguaggiato and M. Valenza (2001a). Hydrogeochemistry and stable isotopes of the thermal springs: earthquake-related chemical changes along Belice Fault (Western Sicily). *Appl. Geoc.*, 00, 1-17.
- Favara, R., S. Francofonte, F. Grassa, M. Liotta, F. Proietto, G. Riccobono and M. Valenza (2001b). Studio idrogeochimico degli acquiferi presenti nell'area della Riserva Naturale "Grotta di Santa Ninfa". *Naturalista sicil.*, S. IV, XXV (Suppl.), 237-254.
- Favara, R., F. Grassa, P. Madonia and M. Valenza (2007). Flow changes and geochemical anomalies in warm and cold springs associated with the 1992-1994 seismic sequence at Pollina, Central Sicily, Italy. *Pure and Appl. Geophys.*, 164, 12, 2411-2430.
- Gonfiantini, R., M.A. Roche, J.C. Olivry, J.C. Fontes and G.M. Zuppi (2001). The altitude effect on the isotopic composition of tropical rains. *Chem. Geol.*, 181, 147-167.
- Liotta, M., F. Grassa, W. D'Alessandro, R. Favara, E. Gagliano Candela, A. Pisciotta and C. Scaletta (2013). Isotopic composition of precipitation and groundwater in Sicily, Italy. *Appl. Geochem.*, 34, 199-206.
- Longinelli, A. and E. Selmo. Isotopic composition of precipitation in Italy: a first overall map. *J. Hydrol.*, 270, 75-88.
- Madonia, P. (2001). Problematiche cartografiche ed idrogeologiche relative alla ripermutazione della Riserva Naturale "Grotta di Santa Ninfa". *Naturalista Sicil. S. IV, XXV (Suppl.)*, 227-236.
- Madonia, P. and M. Panzica La Manna (1987). Fenomeni carsici ipogei nelle evaporiti in Sicilia – Grotte d'Italia, 4, XIII, 163-169.
- Madonia, P. and G. Madonia (2020). The "La Grotta" karst system (Santa Ninfa, Belice Valley): hydrogeochemical features and relationships with neotectonics. *Ann. Geophys.*, this volume.
- Madonia, P., P. Cusano, I.S. Diliberto, and M. Cangemi (2013). Thermal anomalies in fumaroles at Vulcano island (Italy) and their relationship with seismic activity. *Phys. Chem. Earth* 63, 160-169.
- Madonia, P., M. Bracci, M. Cangemi, G. Casamento and F.P. Di Trapani (2017). Geo-datasets ed eterogeneità delle fonti cartografiche originarie: il caso del S.I.T. delle cavità naturali nell'area della Riserva Naturale Integrale "Grotta di Santa Ninfa" (TP). XXI ASITA Conference paper, 715-720.
- Marcelli, L. and G. Pannocchia (1971). Uno studio analitico sui dati ipocentrali di 10 terremoti avvenuti in Sicilia occidentale nel Gennaio del 1968. *Annali di Geofisica*, 24 (2), 287-306.
- Martin, J. B., Kastner, M., Henry, P., Le Pichon, X. and S. Lallemand (1996). Chemical and isotopic evidence for sources of fluids in a mud volcano field seaward of the Barbados accretionary wedge, *J. Geophys. Res.*, 101, 20325-20345.
- Michetti, A.M., F. Brunamonte and L. Serva (1995). Paleoseismological evidence in the epicentral area of the January 1968 earthquakes, Belice, southwestern Sicily, in *Perspectives in Paleoseismology*, A.E.G. Spec. Publ., vol. 6, edited by L. Serva and D. B. Slemmons, 127-139, Peanut Butter Publ., Seattle, Wash.
- Mook, W.G. (Ed.) (2000). *Environmental Isotopes in the Hydrological Cycle Principles and Applications*. UNESCO, Paris.
- Parkhurst, D.L. and C.A.J. Appelo (2013). Description of input and examples for PHREEQC version 3—A computer program for speciation, batch-reaction, one-dimensional transport, and inverse geochemical calculations: U.S. Geological Survey Techniques and Methods, book 6, chap. A43, 497 p., available only at <http://pubs.usgs.gov/tm/06/a43>.
- Rovida, A., R. Camassi, P. Gasperini and M. Stucchi (2011). CPTI11, The 2011 Version of the Parametric Catalogue of Italian Earthquakes, Milano, Bologna. <http://emidius.mi.ingv.it/CPTI>
- Ruggieri, G. and G. Torre (1974). Geologia delle zone investite dal Terremoto del Belice. 1) La tavoletta Gibellina. *Rivista Mineraria Siciliana*, XXIV, 139-147 (1973), 27-48.

## **S. Ninfa aquifer: geochemical signature**

**\*CORRESPONDING AUTHOR: Marianna CANGEMI,**

Istituto Nazionale di Geofisica e Vulcanologia,

Palermo (Italia);

e-mail: [marianna.cangemi@ingv.it](mailto:marianna.cangemi@ingv.it)

© 2020 the Istituto Nazionale di Geofisica e Vulcanologia.

All rights reserved